Analysis of ultraviolet photoconductivity in ZnO films prepared by unbalanced magnetron sputtering

doi: 10.1063/1.1558994

Analysis of ultraviolet photoconductivity in ZnO films prepared by unbalanced magnetron sputtering

Parmanand Sharma[a] and K. Sreenivas
Department of Physics and Astrophysics, University of Delhi, Delhi-110007, India

K. V. Rao
Department of Materials Science, Tmfy-MSE, The Royal Institute of Technology, SE 100 44 Stockholm, Sweden

(Received 29 April 2002; accepted 14 January 2003)

Photoresponse characteristics of polycrystalline ZnO films prepared by the unbalanced magnetron sputtering technique have been analyzed for ultraviolet photodetector applications. Changes in the crystallographic orientation and the microstructure of the films due to *in situ* bombardment effects during film growth have been studied. Variations in photoresponse are correlated with the observed changes in the optical properties and the defect concentration in the films. ZnO films with (100) and (101) orientation possessing a small grain size exhibited a slow response with a rise time $=1.99$ s, whereas porous ZnO films with a mixed orientation (100), (002), and (101) and a larger grain size exhibited a fast response speed with a rise time$=792$ ms. The influence of trap levels on the slow and fast rising components of the photoresponse characteristics and the origin for a fast and a stable response have been identified. A slow rise in the photocurrent directly relates to the adsorption and desorption of oxygen on the film surface, and the fast rise is due to a bulk-related phenomena involving embedded oxygen. The magnitude of the photocurrent and the rise time are found to decrease considerably with increasing number of trap levels. © *2003 American Institute of Physics.* [DOI: 10.1063/1.1558994]

I. INTRODUCTION

Detection of ultraviolet (UV) radiation is becoming important in a number of areas such as environmental monitoring, space research, missile warning systems, and high-temperature flame detection.[1] The most common UV detectors currently in use are the photomultiplier tubes (PMT's) and the silicon photodetectors, but they are not solar blind and require costly filters to attenuate unwanted visible and infrared (IR) radiation. There is a need for solid-state UV photodetectors that can be fabricated cost effectively into high-density arrays.[2] Wide-band-gap materials like diamond, silicon carbide (SiC), gallium nitride (GaN), zinc sulphide (ZnS), and zinc oxide (ZnO) are being investigated extensively for selective UV photodetector applications, and thin films of these materials offer an attractive possibility for developing integrated optoelectronic devices.

The transient photoresponse of ZnO thin films in the ultraviolet region has generated a lot of interest and the UV photoresponse in ZnO films was first observed by Mollow[3] in the 1940s. Since then, photoconductivity in ZnO films and metal–semiconductor structures have been extensively investigated. ZnO-based Schottky barrier detectors do exhibit a fast response speed (μs),[4,5] but their fabrication demands stable ultrathin metallic contacts with good ultraviolet transmission properties. In contrast simple photoconducting layers have often displayed a moderate photoresponse with slow rise and decay times.[6] Photoresponse characteristics of polycrystalline ZnO films deposited by ion beam sputtering,[7] chemical methods,[8] rf sputtering,[9–12] metal-oxide chemical vapor deposition (MOCVD),[13] and spray pyrolysis[14] have been widely reported. A slow response time (few seconds to minutes) and a slow recovery to the initial state[6] ranging from a few seconds to several hours and degradation with time[10] are commonly observed. Dependence on film thickness,[15] crystallographic orientation,[9] grain size, post-deposition annealing treatment in H_2/oxygen,[6] doping effects with nitrogen,[10] and the presence of micropores in the films[12] are found to influence the photoresponse characteristics significantly.

Defect concentrations in the films and the influence of dopants are also found to influence the thin-film material properties and the photoresponse. For example, a long response time of thousands of seconds in as-grown diamond films could be reduced to a few seconds by an appropriate post treatment.[16,17] The improvement was related to the identification of different recombination and trapping mechanisms that were closely linked with the structural defect and impurity content in the films. Mg doping in ZnO films has shown a significant increase in the band gap from 3.3 to 4.05 eV, and metal–semiconductor–metal structures with epitaxial $Mg_{0.34}Zn_{0.66}O$ films exhibited a peak response at 308 nm with a fast rise time of 8 ns.[18] However, the large fall time (1.4 μs) has been attributed either to the presence of trap states generated during the processing of the device or the interface states due to phase separation, or compositional fluctuation in the films.

The influence of defects and the beneficial role of dopants on the UV photoresponse of ZnO have not been studied in detail. Recently we reported on the improved photore-

[a]Author to whom correspondence should be addressed. Electronic mail: sharmap@ndb.vsnl.net.in

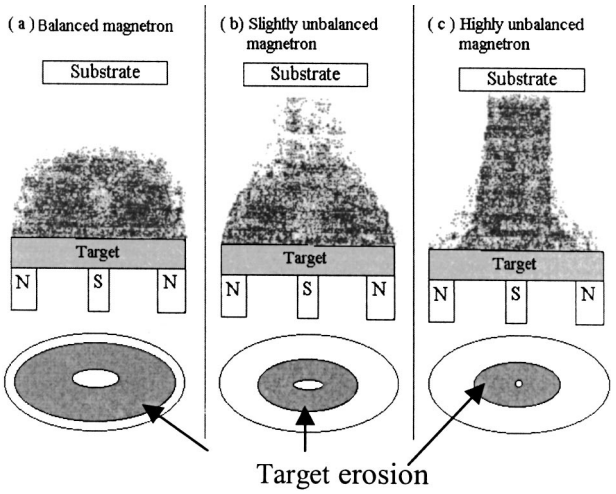

FIG. 1. Plasma confinement and target erosion patterns with a (a) balanced magnetron, (b) slightly unbalanced magnetron (SUM), and (c) highly unbalanced magnetron (HUM) electrode configurations.

sponse characteristics of porous ZnO thin films prepared by an unbalanced magnetron sputtering technique.[19] Significant changes in the microstructure and a varying defect content in the films were noticeable due to *in situ* substrate bombardment effects during growth. In the present paper the observed changes in the structural, optical, and transient photoresponse characteristics have been correlated, and the influence of trap energy levels on the response speed is shown to be significant.

II. EXPERIMENT

Zinc oxide films were deposited by an unbalanced rf magnetron sputtering technique using three different magnetron electrode configurations, which resulted in varying profiles of plasma density as shown in the Figs. 1(a), 1(b), and 1(c). The unbalanced conditions were obtained by progressively lowering the strength of the central magnet in the magnetron electrode to control the ionic flux and the electron bombardment on the substrate.[20] A very weak central magnet [Fig. 1(c)] resulted in intense bombardment effects on the substrate, and the target erosion occurred only in the center. A metallic zinc target was reactively sputtered in argon and oxygen gas mixture, and the influence of deposition parameters on the crystallographic orientation of ZnO films is summarized in Table I. A Phillips x-ray diffraction system was used to examine the crystallite orientation. Surface topography and the internal microstructure of the films were studied using atomic force microscopy (AFM) and scanning electron microscopy (SEM). A double-beam spectrophotometer was used to study the optical properties. Photocurrent was measured on approximately 1-μm-thick ZnO films under varying intensity of UV light ($0.6-32$ mW/cm^2, $\lambda = 365$ nm). Aluminum contacts (3 mm apart) were vacuum evaporated on to the films in the planar configuration for electrical measurements. Photoresponse characteristics were measured at room temperature with a bias voltage of 9.4 V using a Keithley microvolt ammeter (model 150B) and a Tektronix digital oscilloscope (model TDS 310).

III. RESULTS

A. Structural properties

A balanced magnetron electrode producing minimal bombardment effects on the substrate yielded highly *c*-axis-oriented (002) ZnO films as shown in the x-ray diffractogram [Fig. 2(a)]. However, with a slightly unbalanced magnetron (weak central magnet), the degree of *c*-axis orientation was disturbed with the appearance of (100) and (101) orientation [Fig. 2(b)]. When the strength of the central magnet was further weakened the preferred *c*-axis orientation completely disappeared [Fig. 2(d)]. The observed changes in crystallographic orientation by unbalancing the magnetic field were similar to earlier observations of Tominaga *et al.*,[21] where increased bombardment effects by high-energy neutrals were shown to disturb the *c*-axis orientation in dc-magnetron-sputtered ZnO films. Similar bombardment effects were suspected in the present study, and the flux of high-energy neutrals bombarding the substrate in the unbalanced magnetron sputtering process was found to depend on the sputtering

TABLE I. Influence of sputtering conditions on the crystallographic orientation and photoresponse of the films.

Sample	Magnetron configuration	Sputtering power (W)	T-S[a] distance (cm)	Sputtering pressure (mTorr)	FWHM (100)	FWHM (002)	FWHM (101)	Photoresponse rise time (ms)
A	BM[b]	300	10	10	---	0.500	---	No photoresponse
B	BM[b]	150	20	6	---	0.535	---	
C	SUM[c]	200	8	25	0.897	0.556	1.031	
D	SUM[c]	250	8	20	0.962	0.325	1.051	
E	SUM[c]	300	8	15	1.149	0.753	1.063	
F	SUM[c]	350	4.5	10	0.475	0.346	0.484	792
G	HUM[d]	150	8	10	0.507	---	0.7596	1780
H	HUM[d]	250	8	10	0.758	---	0.717	1990
I	HUM[d]	250	4.5	20	0.519	0.451	0.586	831

[a]Target to substrate.
[b]Balanced magnetron.
[c]Slightly unbalanced magnetron.
[d]Highly unbalanced magnetron.

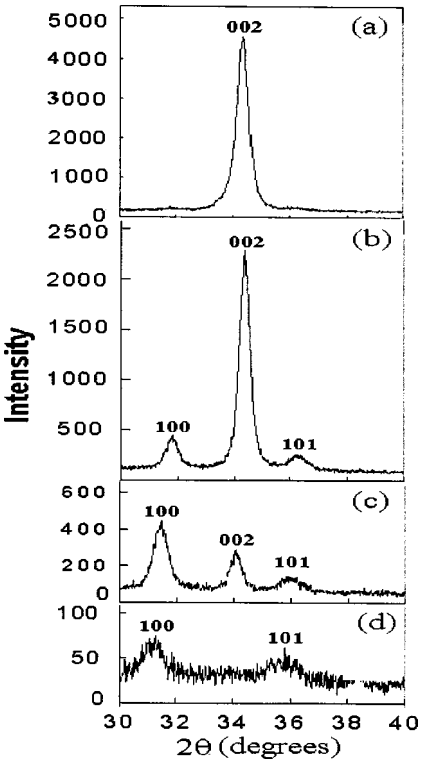

FIG. 2. X-ray diffraction patterns of ZnO films deposited with (a) balanced magnetron, (b) slightly unbalanced (sample F), and (c) highly unbalanced magnetron (sample I), and (d) sample H.

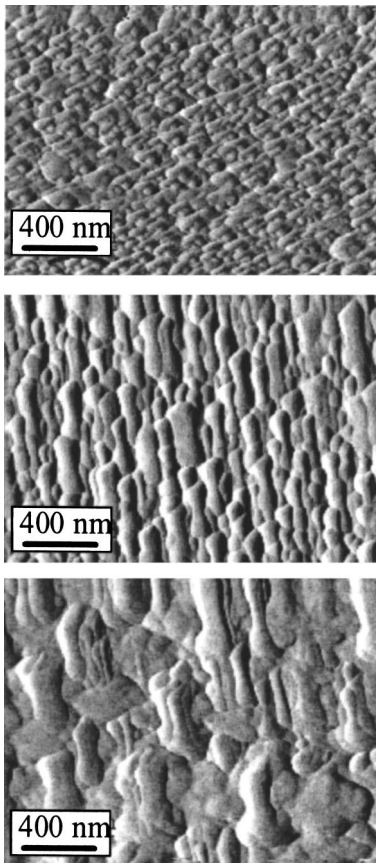

FIG. 3. AFM images of sputtered ZnO thin films (area 2 μm$\times$2 μm): (a) *c*-axis (002)-oriented film, (b) (100)- and (101)-oriented film, and (c) (100), (002), and (101) mixed oriented film.

parameters like power, pressure, and target to substrate distance (Table I). Using a slightly unbalanced magnetron (SUM) electrode produced ZnO films having a (100), (002), and (101) mixed orientation, and with the highly unbalanced magnetron (HUM) electrode films possessing either [(100), (002), (101)] or [(100), (101)] mixed orientations were produced depending upon the sputtering conditions (Table 1). The [(100), (101)] orientation was mostly obtained when the target-to-substrate distance was large (8 cm) and sputtering pressures and power were low (10 mTorr and 150 W). Visual inspection of the ZnO films having [(100), (101)] orientation revealed the films to be highly transparent but the films with a [(100), (002), (101)] mixed orientation always exhibited a characteristic milky appearance, and such films were further examined in detail.

B. Surface topography

Film surface morphology was examined in air with an AFM using a Nanoscope IIIa manufactured by Digital instruments, Inc. All samples were scanned over an area of 2 $\times 2$ μm^2 at several locations, and the changes in the surface topography are shown in Fig. 3. *c*-axis-oriented ZnO film produced with the balanced magnetron revealed round-shaped grains of uniform size [Fig. 3(a)] in contrast to the elongated grain structure of the mixed oriented films [Figs. 3(b) and 3(c)]. Films possessing the (100), (002), and (101) mixed orientation were relatively rough with a mean roughness of 12.17 nm in comparison to the highly *c*-axis-oriented and (100), (101)-oriented films which had a mean roughness of 5.817 and 5.940 nm. Chemically etched thin-film cross sections were prepared to examine the internal microstructure in the bulk of the film by SEM. A porous microstructure was observed for the (100), (002), and (101) mixed oriented films as shown in Fig. 4(a), in contrast to the dense columnar structure [Fig. 4(b)] of highly *c*-axis-oriented ZnO films.

C. Optical properties

Optical transmission and absorption spectra of ZnO thin films were recorded at room temperature in the wavelength range of 350–800 nm using a Varian (Cary 100 BIO) double-

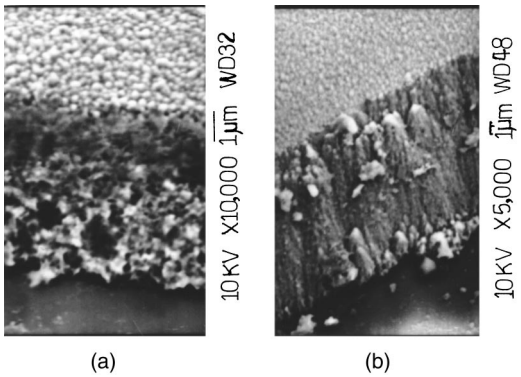

FIG. 4. Scanning electron micrographs showing internal microstructure of the films: (a) porous structure of (100), (002), and (101) mixed oriented films and (b) dense columnar structure of *c*-axis-oriented ZnO films.

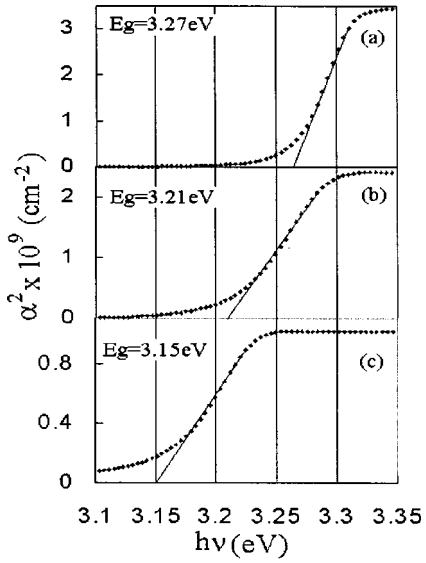

FIG. 5. Variation in absorption coefficient with photon energy: (a) *c*-axis (002)-oriented film, (b) (100)- and (101)-oriented ZnO film, and (c) (100), (002), and (101) mixed oriented film.

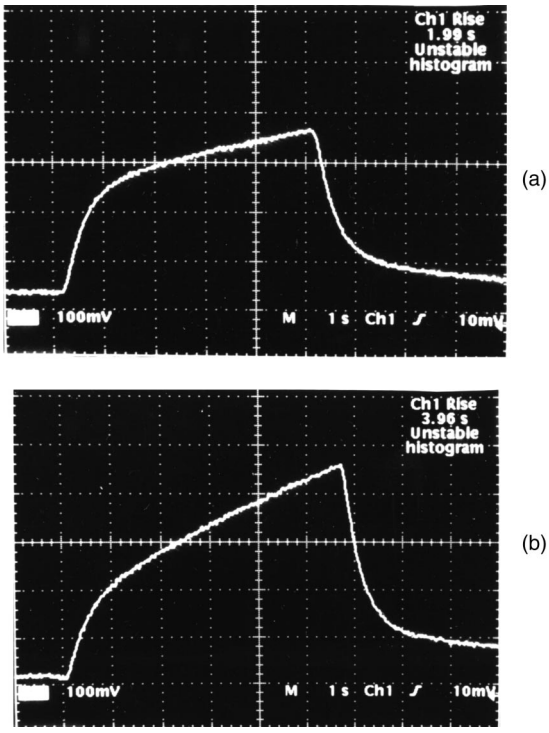

FIG. 6. Photoresponse curves of ZnO thin films having (100) and (101) crystallite orientations: (a) UV intensity=9.5 mW/cm^2 (scale: *x* axis: 1 s/div.; *y* axis: 100 mV/div.) (b) UV intensity=19 mW/cm^2 (scale: *x* axis: 1 s/div.; *y* axis: 100 mV/div.)

beam spectrophotometer, with a clean glass substrate in the reference beam. The *c* axis and the [(100), (101)]-oriented films were highly transparent (>90%) but (100)-, (002)-, and (101)-oriented films (<80%) possessed a milky appearance. The absorption coefficient (α) was calculated from the absorbance (A) and the film thickness (d) using the following relation:[22]

$$\alpha = 2.303 \times (A/d). \tag{1}$$

The energy gap (E_g) was obtained by extrapolating the linear part of the α^2 versus $h\nu$ plot (Fig. 5). A band gap of 3.27 eV for the *c*-axis-oriented ZnO film was found to be close to the reported values in the literature (3.29 eV) (Ref. [23]) and ZnO films with orientation [(100), (101)] and a mixed [(100), (002), (101)] were found to have lower values of 3.21 eV and 3.15 eV, respectively.

D. Ultraviolet photoresponse

c-axis-oriented ZnO films did not exhibit any appreciable photoresponse. Films possessing (100) and (101) mixed crystallite orientation [Fig. 3(b)] exhibited a large photocurrent change (15.36 μA cm^2/W) with a slow rise and a slow recovery to the initial value. The typical photoresponse profile is shown in Fig. 6(a). As the intensity of UV light is increased from 9.5 to 19 mW/cm^2, the rise time increased from 1.99 to 3.96 s, respectively [Figs. 6(a) and 6(b)]. These samples when tested in vacuum (10^{-3} mTorr) exhibited a continuous increase in photoconductance and exhibited saturation after a long time (minutes). When the UV light was switched off recovery to the initial state was incomplete and the decay was very slow in vacuum.

In contrast a drastically reduced photocurrent (2.75 μA cm^2/W) was observed in ZnO films possessing (100), (002), and (101) mixed crystallite orientations, but the response time was relatively fast (792 ms). Complete recovery to initial value was observed with a fast fall time of 805 ms [Fig. 7(a)]. No appreciable change in the rise and fall time was observed with the increase in the intensity of UV light, and a reproducible response to pulsed UV light is shown in Fig. 7(b). These films showed little degradation with time even after 6 months when left in air at room temperature, and only a slight change [Fig. 7(c)] was observed in the rise time (=962 ms) and the recovery time (=974 ms). When tested in vacuum they did not show any appreciable change in the response characteristics. A good linearity was observed in the photocurrent versus UV intensity characteristics (Fig. 8). In general the sensitivity was high for films possessing a smaller grain size with (100) and (101) orientation in comparison to films having the (100), (002), and (101) mixed orientation, and the responsivity increased with shorter electrode spacing without affecting the rise and the fall time.

IV. THEORY

Photoconduction in ZnO thin films is primarily governed by desorption and adsorption of oxygen originating either from a bulk related, or a surface related process.[10] The surface-related process is slow, and in the absence of UV light, oxygen is adsorbed by taking a free electron from the surface of the *n*-type ZnO to form a chemically adsorbed surface state, leaving behind a depletion region near the surface of the film.[15] If the film is thin, the depletion region can extend through the entire width of the film:

$$O_2 + e^- \rightarrow O_2^- . \tag{2}$$

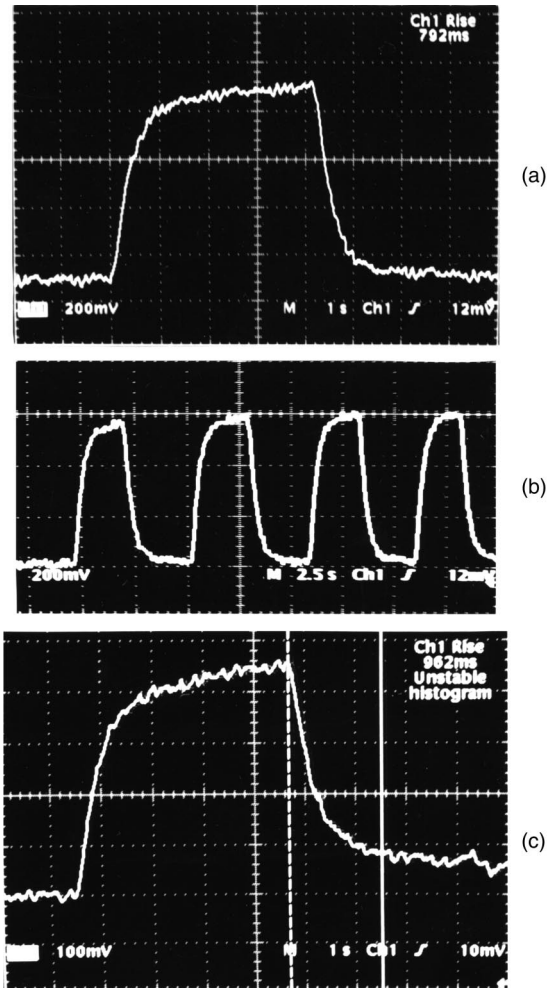

FIG. 7. Photoresponse of ZnO thin films having (100), (002), and (101) mixed crystallite orientations at UV intensity = 9.5 mW/cm^2: (a) fresh film (scale: *x* axis: 1 s/div.; *y* axis: 100 mV/div.) (b) pulse response of (a) (scale: *x* axis: 2.5 s/div.; *y* axis: 200 mV/div.), and (c) six month old (scale: *x* axis: 1 s/div.; *y* axis : 100 mV/div.)

When photons of energies higher than the fundamental absorption band of ZnO are incident, holes produced by the light adsorption near the surface discharge the negatively charged oxygen ions:

$$h^+ + O_2^- \rightarrow O_2(g). \tag{3}$$

Electrons produced at the same time increase the conductivity of the film. The decay in photoconductivity is therefore strongly dependent on the ambient gas conditions.

In the bulk-related process excess oxygen chemisorbed at the grain boundaries of the crystallite behaves in the same way as the oxygen chemisorbed on the free surface of ZnO. This process introduces a barrier, and when irradiated with UV light, the barrier height is lowered and an increase in the conductivity is observed.[10] The photodesorbed oxygen at the grain boundaries in the bulk is quickly chemisorbed again in the absence of UV light. Since the process is happening in the bulk of the material, it results in a faster response, and it is not influenced by the ambient gas conditions.

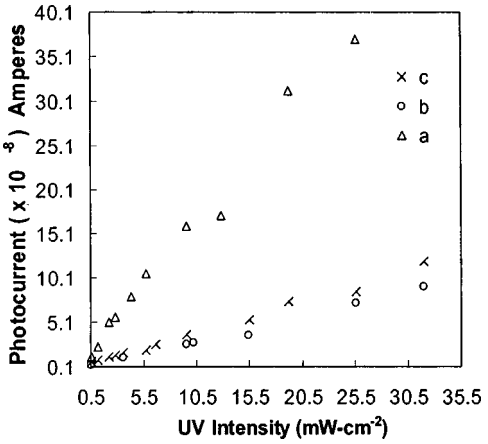

FIG. 8. Variation of photocurrent with UV light intensity for ZnO films having different crystallite orientations: (a) (100) and (101) orientations [△], (b) (100), (002), and (101) orientation [○], and (c) data on a six month old [×] sample of "b."

V. DISCUSSION

A. Structure, composition, and defect nature in ZnO films

The normal growth habit of sputtered ZnO films is along a preferred (002) *c*-axis orientation with a balanced magnetron electrode. However, with the unbalanced magnetron sputtering process significant changes in the structural properties were observed [Figs. 2(b), 2(c), and 2(d)], and these could be correlated with the energy and flux of sputtered specie bombarding the growing film. In the HUM where the plasma is very dense between the target and the substrate [Fig. 1(c)], the energy and flux of ions and neutrals bombarding the film surface is very high. Sticking probability of oxygen neutrals in the growing film and the defect concentration in the bulk of the film were expected to be low.[24] However, the intense resputtering effects due to the high flux of ions and neutrals are found to disturb the preferred (002) *c*-axis orientation, and the nucleation of the (100)- and (101)-oriented crystallites tends to dominate [Figs. 2(c) and 2(d)].[21] It may be noted from Table I that under the highly unbalanced mode of sputtering (HUM) as the target to substrate distance decreases to 4.5 cm and the sputtering pressure increases to 20 mTorr, the energy of ions and neutrals bombarding the film decreases, due to increased number of collisions at higher pressures, and produced films with a mixed [(100), (002), and (101)] orientation. In case of the SUM of sputtering where the energy and flux of ions bombarding the substrate are low, the ZnO films possessed commonly a mixed (100), (002), and (101) orientation [Fig. 2(b)] and had a milky appearance irrespective of the deposition parameters (Table I). The chances of containing embedded oxygen in these films was considered high due to the reduced energy of the bombarding specie, and a high density of trapped oxygen neutrals, or defects, was expected. In the case of the balanced mode of sputtering the flux and the energy of ions bombarding the film are at a minimum, and films are highly (002) *c*-axis oriented [Fig. 2(a)] with a minimum number of defects.

The stoichiometry of three representative samples having [(100), (101)] orientation, [(101), (002), (101)] oriented in which (002) orientation was very weak, and a [(100), (002), (101)]-oriented film with a dominant (002) crystallite orientation was analyzed by elastic recoil detection analysis (ERDA). Films possessing [(100) (101)] crystallite orientation (sample H) was found to have high concentration of Zn, and the compositional ratio Zn/O=3.2. The excess Zn concentration was found to reduce with the appearance of the (002) orientation and Zn/O=1.27. However, the [(100), (002) (101)] mixed oriented films [Fig. 2(b)] were found to contain excess oxygen with Zn/O=0.95. This was contrary to the expectation because ZnO is a well-know *n*-type semiconductor, and the presence of excess oxygen could be only due embedded oxygen neutrals at the grain boundary. Kim and Kim[25] have also observed excess oxygen in ZnO films deposited by plasma-enhanced chemical vapor deposition and were detected mainly in the grain boundary region.

The nature of native defects present in the Zn-rich and O-rich films obtained in the present work could be understood from the analysis presented by Zhang *et al.*[26] In the case of Zn-rich films *n*-type behavior is identified with the shallow donor levels generated by (i) oxygen vacancy (V_O), (ii) contribution from Zn-on-O antisite (Zn_O), and (iii) the dominant presence of abundant Zn interstitial (Zn_i) under both Zn-rich and O-rich conditions because its formation enthalpy is very low. Presence of oxygen interstitials (O_i) and zinc vacancy (V_{Zn}) was not expected in the Zn-rich films since their formation enthalpy was very high. However, in the O-rich films, acceptors like oxygen interstitial (O_i) and the zinc vacancy (V_{Zn}) were expected, forming shallow levels with respect to the valence band (or deep with respect to conduction band), readily producing holes that could act as electron killers or as a recombination center for the electrons.

B. Surface topography and related photoresponse

The AFM studies revealed a small grain size (164 $\times$87 nm) in the (100)- and (101)-oriented film [Fig. 3(b)] in comparison to (100), (002), and (101) mixed oriented ZnO film [Fig. 3(c)]. In films with a smaller grain size chemisorbed oxygen on the surface is expected to be more due to the large number of grain boundaries, and consequently a large change in photoconductance is observed in the presence of UV light. The chemisorption of oxygen could have occurred in these films when they were first exposed to air soon after the growth. The photoresponse curves shown in Figs. 6(a) and 6(b) clearly indicate that the origin for the photocurrent generation is related to two different processes. The transition from one process to another is observed more clearly in [Fig. 6(b)], when the films are illuminated with UV light at a higher intensity. The initial rise in the photocurrent is quite fast and is followed by a slow rise towards a saturation level depending upon the intensity of illumination. The fast initial rise in the conductivity is attributed to a bulk-related process, and the slow variation could originate from a surface-related phenomenon involving desorption of oxygen under ultraviolet light and chemisorption of oxygen in the absence of UV light. Moreover, as ZnO itself is half oxygen, a minute change in stoichiometry can also contribute to oxygen at the grain boundaries on the surface of the film. Numerous photoactive states due to dangling bonds at the grain boundary interface are possible, and a surface-related photoconductivity seems to overwhelm any bulk photoconductivity. This was further confirmed by testing the samples in vacuum. A continuous increase in photoconductance was observed and exhibited saturation only after a long time (minutes) due to the continuous removal of chemisorbed oxygen, and in the absence of UV light the decay was very slow and never reached the initial value.

Films with the mixed (100), (002), and (101) orientation revealed a larger grain size (425$\times$169 nm) from the AFM study shown in Fig. 3(c). In these films oxygen chemisorbed on the surface is expected to be small due to the relatively lesser grain boundary region, and more oxygen seems to be trapped in the bulk of the film due to the low intensity of bombardment effects under which these films were grown. Excess oxygen embedded in the film is known to introduce a barrier between the crystallites.[10] The photoresponse occurs due to the lowering of the barrier height at the grain boundaries in the presence of UV light and increases the conductivity of the film. The fast recovery and rise seen in these films [Fig. 7(a)] is purely due to the electronic process (exchange of electrical charge) involving embedded oxygen at the grain boundaries during photodesorption and adsorption. These films did not show any change in the photoresponse when tested in vacuum. The rise time, decay time, and the saturation level were unaffected in vacuum. The photoresponse characteristics were quite reproducible [Fig. 7(c)] when long-term stability tests were carried out on films left in air after 6 months. The cross-sectional SEM image [Fig. 4(a)] also revealed a porous structure in the bulk of the film in contrast to the dense columnar structure for the smooth *c*-axis-oriented film [Fig. 4(b)] and supports a higher defect concentration in the films.

C. Optical properties

In the case of *c*-axis-oriented ZnO films a sharp rise in the absorption coefficient indicated a direct band gap semiconductor and a low defect density [Fig. 5(a)]. However, shrinkage in the band gap value for the mixed oriented ZnO films [Figs. 5(b) and 5(c)] was observed and is attributed to the presence of local strain induced by the nonintentional impurities, point defects, and poor crystallinity.[27] Band gap shrinkage was found to become significant for the films having (100), (002), and (101) mixed orientation (E_g =3.15 eV) in contrast to the film having (100) and (101) mixed orientation (E_g=3.21 eV). A comparison with *c*-axis-oriented film shows that the rise in the absorption coefficient had lower slope for the mixed oriented films. Moreover, for the (100), (002), and (101) mixed oriented ZnO films the absorption coefficient did not reached to zero near the band edge and the variation in α^2 versus $h\nu$ [Fig. 5(c)] exhibited two distinct slopes, indicating intermediate energy levels between the valence band and the conduction band. Such intermediate energy levels are known to act as a trap energy level or a recombination center for the electrons generated in the

presence of UV light.[28] The observed variations in the optical data and the O-rich nature of the (100), (002), and (101) mixed oriented films clearly suggested a higher trap level density in the bulk of the film and the presence of oxygen interstitials and neutrals.

D. Effect of traps on photoresponse speed

The transient behavior of ZnO thin films prepared by the unbalanced mode of sputtering seems to be governed by intermediate energy levels present between the valence and the conduction band, known as traps or the recombination centers. The presence of large number of traps can reduce the photocurrent by capturing the charge carriers (electrons) and also result in a fast equilibrium between the rate of generation and recombination of charge carriers that leads to the fast photoresponse. The trap energy levels (M) lying near the conduction band edges have higher probability of becoming trapping center also known as shallow traps, while the traps in the middle of the forbidden band act more likely as a recombination centers (S). If the traps are shallow with few, or no, recombination centers, then band electron recombine through trapping levels. Such recombination is a slow process because trapped electrons return back to the conduction band many times before they manage to recombine.

The change in electron density in the conduction band per unit time may be written as[29]

$$\frac{dn}{dt} = k\beta I - \gamma_n n(N_{cM} + M) + \beta k I \gamma_n N_{cM} t, \tag{4}$$

where k, l, β, and M are the optical absorption coefficient, light intensity, quantum yield, and number of trap energy levels, respectively. The product $\gamma_n N_{cM}$ is the return probability of an electron from a trap energy level (M) to the conduction band. The solution of differential equation (4) has the form

$$n = \beta k I[\gamma_n M \theta^2 (1 - e^{(-t/\theta)}) + \gamma_n N_{cM} \theta t], \tag{5}$$

where

$$\theta = \frac{1}{\gamma_n (M + N_{cM})}. \tag{6}$$

The solution of Eq. (4) is the sum of an exponential and a linear term, and the shape of the photoresponse curve depends on the number of trap energy levels [Fig. 9(a)]. It is found that photoresponse curve has two different slopes that are separated from each other at $(t) \approx \theta$. As the number of trap energy levels (M) decreases from M_4 to M_0 as shown in Fig. 9(a) the slope of the second part approaches the initial slope. The initial part of the curve up to $t \approx \theta$ is not affected by the recombination or trapping, and during the time θ, equilibrium is established between the conduction band and the trap energy levels (M), and the subsequent relaxation in the electron density (n) occurs under approximately equilibrium conditions. After $t > \theta$, a fraction of electrons $[N_{cM}/(M + N_{cM})]$ excited to the upper band are in the conduction band and the remaining electrons are at the M levels.

The experimentally observed response was fitted to Eq. (5) and the value of $\theta = 0.531$ s was noted from the experimental curve shown earlier in Fig. 7(a) for the (100), (002), and (101) mixed oriented film shown in Fig. 9(b). After $t > \theta$, only 0.12% of the electron are present in the conduction band with a return probability ($\gamma_n N_{cM}$) $= 2.2 \times 10^{-3}$ back to the conduction band [Fig. 10(b)] from the M levels. However, fitting of photoresponse curve of Fig. 6(a) for the [(100) (101)]-oriented film shown in Fig. 9(c) indicated an increase in the percentage of electron (3.54%) and return probability ($\gamma_n N_{cM} = 9.1 \times 10^{-2}$) as well at the same intensity of UV radiation (of 9.5 mW/cm^2) and resulted in a slow rise in response after $t > \theta$. When the intensity of UV illumination increased to 19 mW/cm^2, the electrons present in the conduction band (51.47%) and their return probability ($\gamma_n N_{cM} = 9.4 \times 10^{-1}$) further increased without affecting the slope of the initial rise. While no appreciable change was observed in the photoresponse curve for (100), (002), and (101) mixed oriented ZnO thin films with UV intensity.

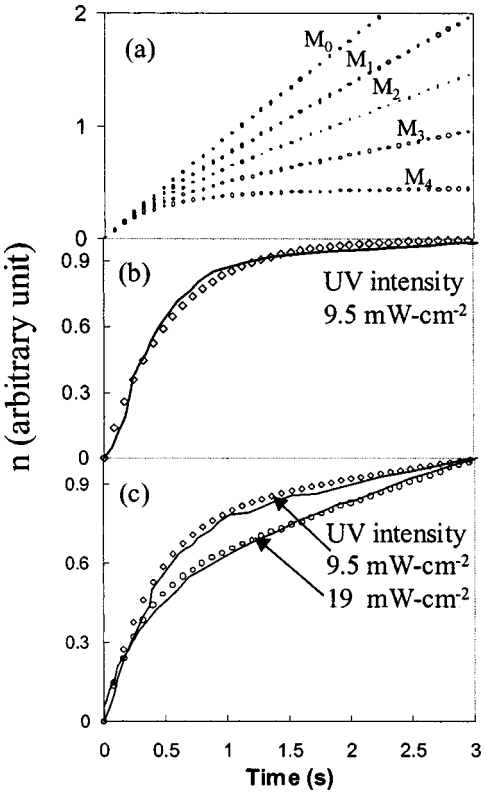

FIG. 9. Variation in the rise of photoconductivity due to the presence of trapping levels (solid curve represents experimental response, and points on the curve show theoretical fitting): (a) theoretical curves for increasing number of tapping levels ($M_0 < M_1 < M_2 < M_3 < M_4$), (b) fitting the experimental photoresponse rise (100), (002), and (101) mixed oriented ZnO film, and (c) a theoretical fit for the response from (100)- and (101)-oriented ZnO film at two different level of illumination.

The photoresponse decay characteristics for the [(100), (101)]-oriented Zn-rich films and the (100)-, (002)-, and (101)-oriented O-rich films are compared in Fig. 10. Initially a fast decay is observed, and the slope is found to be nearly the same irrespective of nature and orientation of the film and the intensity of UV illumination. There was no change with the illumination level for the [(100), (101)]-oriented ZnO films and they exhibited a slow relaxation in photoconductivity. However, the decay was relatively faster in case of

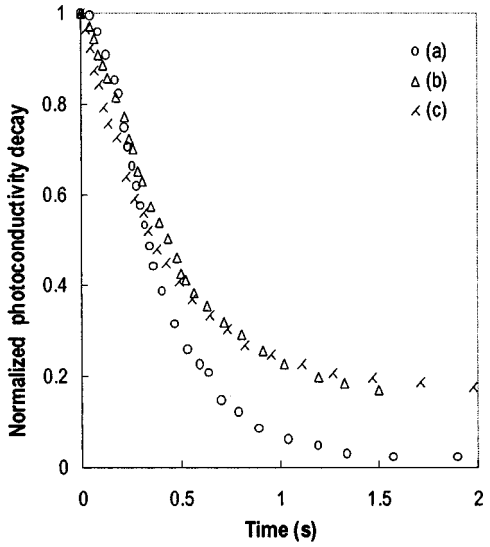

FIG. 10. Photoresponse decay curve for ZnO films having different crystallite orientations: (a) (100), (002), and (101) at UV intensity 9.5 mW/cm^2 [○], (b) (100) and (101) oriented at UV intensity of 9.5 mW/cm^2 [△], and (c) for sample (b) at UV intensity 19 mW/cm^2 [×].

O-rich films, and the recovery to the initial state was complete. The slow relaxation in Zn-rich could be well explained due to the presence of shallow traps created by zinc interstitial and the fast decay in O-rich films due to deep traps created by oxygen interstitials in the bulk of the film.

VI. CONCLUSIONS

Micro structural changes due to the inherent bombardment effects in an unbalanced magnetron sputtering process produce ZnO films that are either Zn rich or O rich. The response speed and the ultraviolet photoresponse characteristics are different for these films and seem to be governed by the types of native defects present in the film. Theoretical analysis shows that the rise in photoconductivity in ZnO is governed by the trap energy levels as generated by the native defects. Films with [(100), (101)] orientation containing excess Zn exhibited a slow response and are related to the shallow traps created mainly by zinc interstitials. However, porous ZnO films with (100), (002), (101) mixed orientation that were O rich had a characteristic milky appearance exhibited a fast response. Excess oxygen embedded at the grain boundaries in the porous microstructure of the film is found to create deep traps. In these films, although the magnitude of the photocurrent reduced, the response was relatively faster due to a bulk-related process, and films exhibited reproducible characteristics with minimum degradation.

ACKNOWLEDGMENTS

The authors are thankful to Professor Abhai Mansingh for fruitful discussions. The authors thank Dr. D. K. Avasthi of Nuclear Science Center, Delhi for the ERDA experiments.

[1] P. Schreiber, T. Dang, G. Smith, T. Pickenpaugh, P. Gehred, and C. Litton, Proc. SPIE **3629**, 230 (1999).
[2] J. C. Carrano, T. Li, P. A. Grudowski, R. D. Dupuis, and J. C. Cambell, Circuits & Devices, 15 (1999).
[3] E. Mollow, in *Proceedings of the Photoconductivity Conference*, edited by R. G. Breckenridge (Wiley, New York, 1954), p. 509.
[4] H. Fabricius, T. Skettrup, and P. Bisgaard, Appl. Opt. **25**, 2764 (1986).
[5] Y. Liu, C. R. Gorla, S. Liang, N. Emanetoglu, Y. Lu, H. Shen, and M. Wraback, J. Electron. Mater. **29**, 69 (2000).
[6] S. A. Studenikin, N. Golego, and M. Cocivera, J. Appl. Phys. **87**, 2413 (2000).
[7] D. H. Zhang and D. E. Brodie, Thin Solid Films **238**, 95 (1994).
[8] A. M. Fernandez and P. J. Sebastian, J. Phys. D **26**, 2001 (1993).
[9] D. H. Zhang and D. E. Brodie, Thin Solid Films **251**, 151 (1994).
[10] D. H. Zhang, J. Phys. D **28**, 1273 (1995).
[11] H. Y. Kim, J. H. Kim, M. O. Park, and S. Im, Thin Solid Films **398–399**, 93 (2001).
[12] H. Y. Kim, J. H. Kim, Y. J. Kim, K. H. Chae, C. N. Whang, J. H. Songand, and S. Im, Opt. Mater. **17**, 141 (2001).
[13] S. Liang, H. Sheng, Y. Liu, Z. huo, Y. Lu, and H. Shen, J. Cryst. Growth **225**, 110 (2001).
[14] S. A. Studenikin, N. Golego, and M. Cocivera, J. Appl. Phys. **87**, 2413 (2000).
[15] Y. Takahashi, M. Kanamori, A. Kondoh, H. Minoura, and Y. Ohya, Jpn. J. Appl. Phys., Part 1 **33**, 6611 (1994).
[16] S. Salvatori, M. C. Rossi, and F. Galluzi, IEEE Trans. Electron Devices **47**, 1334 (2000).
[17] R. D. McKeag and R. B. Jackman, Diamond Relat. Mater. **7**, 515 (1998).
[18] W. Yang, R. D. Vispute, S. Choopun, R. P. Sharma, T. Venkatesan, and H. Shen, Appl. Phys. Lett. **78**, 2787 (2001).
[19] P. Sharma, A. Mansingh, and K. Sreenivas, Appl. Phys. Lett. **80**, 553 (2002).
[20] B. Window and N. Savvides, J. Vac. Sci. Technol. A **4**, 196 (1986).
[21] K. Tominaga, N. Ueshiba, Y. Shintani, and O. Tada, Jpn. J. Appl. Phys., Part 1 **20**, 519 (1981).
[22] F. Jahan, M. H. Islam, and B. E. Smith, Sol. Energy Mater. Sol. Cells **37**, 283 (1995).
[23] F. Quaranta, A. Valentini, F. R. Rizzi, and G. Casamassima, J. Appl. Phys. **74**, 244 (1993).
[24] C. R. Aita, R. J. Lad, and T. C. Tisone, J. Appl. Phys. **51**, 6405 (1980).
[25] Y. J. Kim and H. J. Kim, Mater. Lett. **41**, 159 (1999).
[26] S. B. Zhang, S. H. Wei, and A. Zunger, Phys. Rev. B **63**, 075205 (2001).
[27] A. Tiburcio-Silver, J. C. Joubert, and M. Labeau, J. Appl. Phys. **76**, 1992 (1994).
[28] R. H. Bube, *Photoelectronic Properties of Semiconductors* (Cambridge University Press, Cambridge, England, 1992).
[29] S. M. Ryvkin, *Photoelectric Effect in Semiconductors* (Consultants Bureau, New York, 1964), p. 129.